J Ther Eng, Vol. 7, Supp 14, pp. 1857–1871, December, 2021

Journal of Thermal Engineering
Web page info: https://jten.yildiz.edu.tr
DOI: 10.18186/thermal.1051259

Journal of Thermal Engineering

Research Article

Modeling of the effect of nano-enhanced phase change material on the performance of a large-scale wallboard

Leyli BAHRAMI, Alibakhsh KASAEIAN*, Fathollah POURFAYAZ, Sahar GHAFARIAN

Faculty of New Sciences and Technologies, University of Tehran, Tehran, Iran

ARTICLE INFO

Article history
Received: 03 December 2020
Accepted: 22 April 2021

Key words:
Phase change material; Computational fluid dynamics; Building; Nano-enhanced PCM

ABSTRACT

The main goal of this present study is to investigate the effects of the application of PCM and Nano-enhanced PCM as wallboard on the thermal behavior of a room. For this purpose, a room was modeled in two dimensions under Tehran's summer weather conditions through computational fluid dynamics (CFD). The effect of using the PCM as a wallboard in the southern wall in both pure and enhanced with nanoparticles was investigated. The indoor temperature, the wall surface temperature, and the interior wall heat flux, in both cases, were reported and compared. At the end of this study, the acquired results were compared with the pre-modified room, and thermal improvement was reported. The results indicate that the use of solid nanoparticles in PCM reduces the energy consumption of air-conditioning system by 7.4% compared to the conventional room. In the case of the Nano-enhanced PCM wallboard, the room has better thermal performance than the pure PCM, with 4.37% more energy storage, about 0.273 reductions in temperature decrement factor, and a 21.6 min increase in the time delay to peak temperature. Compared to the conventional room and room with pure PCM, the room's temperature fluctuation, modified by Nano-enhanced PCM, reduces by 52% and 31%, respectively. This study's obtained results could help the researchers and designers have a more appropriate PCM selection for building ventilation system applications.

Cite this article as: Bahrami L, Kasaeian A, Pourfayaz F, Ghafarian S. The temperature distribution of the wet cylinder liner of v-12 engine according to calculation and experiment. J Ther Eng 2021:7:Supp 14:1857–1871.

INTRODUCTION

According to the International Energy Agency (IEA), 36% of the energy consumption and 40% of the total indirect and direct CO2 emissions in the world are driven by building and building construction sectors [1]. Consequently, any efforts for decreasing energy consumption in this sector would be precious. The application of phase change material in buildings would be one of the best solutions for achieving less energy consumption and less CO2 emissions. Utilizing phase change material (PCM), either passive or active, as a thermal energy storage method in building, has a high potential for building energy-saving and indoor

***Corresponding author.**
*E-mail address: akasa@ut.ac.ir

This paper was recommended for publication in revised form by Regional Editor Baha Zafer

Published by Yıldız Technical University Press, İstanbul, Turkey
Copyright 2021, Yıldız Technical University. This is an open access article under the CC BY-NC license (http://creativecommons.org/licenses/by-nc/4.0/).

temperature regulation. The PCMs have been identified as sustainable and environment-friendly materials, which have higher energy storage density and reversibility than the sensible heat storage materials. These materials not only can reduce building energy consumption and maintain the building temperature comfortable but also have benefits in other applications such as distillation and batteries [2–4]. Phase change materials have been applied in the building sector as thermal storage from the beginning of the 1980s [5]. The first study about applying PCMs in buildings was conducted in 1988, which presented a theoretical study on the latent and sensible heat [6]. The PCM-incorporated building materials as wallboard, wall, roof, floor, and venetian blind are appropriate alternatives for thermal energy storage (TES).

In 2010, De Gracia et al. [7] analyzed the environmental effects of applying PCM in building construction in life cycle assessment (LCA) in different climates. The results showed that the application of PCM decreased the energy consumption in a building. Furthermore, they stated that the global benefit of integrating PCM in the building could be maximized in a long-term operation. In another study, Baetens et al. [8] reviewed PCM applications in buildings and found that concrete-enhanced PCM led to a significant increase in the thermal building capacity. Diaconu and Cruceru [9] designed a composite PCM wall system for utilizing in a building. They proved that their proposed system could reduce the annual energy demand for both air-conditioning and heating. Kuznik et al. [10] experimentally studied the thermal performance enhancement of a building with PCM wallboard. Their outcomes proved that adding the PCM wallboard to the building walls and roof enhanced thermal comfort. An experimental study was carried out about the effect of PCM implementation on the output of a photovoltaic thermal (PVT) system [11]. The experimental results revealed that the PCM could increase the electrical efficiency of the PVT by 9 %. Likewise, Amirifard et al. [12] confirmed the positive effects of PCM on a PCM-integrated solar pond's efficiency and thermal behavior via the finite difference method. Finally, they showed that the integration of PCM with the solar pond could improve the solar pond's average efficiency up to 6.1% at the discharging time. To improve the performance of PCMs, using metal fins and forced convection could be positively influential [13]. In this manner, Bai et al. [14] developed and studied a solar thermal storage heating system comprised of several efficient solar collecting heat storage units filled with PCM (low melting point modified paraffin) and finned heat pipe. Ultimately, it was observed that the overall solar energy utilization reached 55% when the average solar radiation was at 998W/m2. As another study in this context, Korti [15] carried out a numerical study of a latent heat storage exchanger filled with paraffin as the PCM. In the PCM container, water was flown by forced convection through tubes, leading to heat transfer within the PCM. Zhou et al. [16] proposed a passive energy technology named PCM-filled earth-air heat exchanger and monitored this system's cooling performance through numerical studies and experiments. The results showed that the proposed unit could achieve a 20.24% improvement in cooling capacity compared to the traditional earth-air heat exchangers.

As an unlimited energy source, the storing of solar energy is one of the most profitable ways to use thermal energy when the sun disappears. On this basis, Ben Zohra et al. [17] proposed a solar system in which a PCM was incorporated in a solar collector. According to the obtained results in this study, the system could store a remarkable amount of solar energy in a shorter time than the other previously proposed systems. In another study, Mousavi et al. [18] investigated the effects of a copper foam filled with paraffin C22 as PCM on a photovoltaic thermal module via CFD simulation. They also studied the effects of various key factors such as inclination, inlet water temperature, mass flow rate, and solar irradiance. Prytania et al. [19] conducted an energetic investigation of three different solar-assisted heat pump underfloor heating systems, with and without PCM layer on the floor. The utilization of PCM in the underfloor heating system reduced 40% heating loads. In another study, the authors investigated a solar cooling system with and without PCM. They carried out a comparative study between various cases in which PCM was placed in each radiant wall. The collected results indicated that incorporating PCM in the southern wall, as the best choice among the four radiant walls, led to 30% in the auxiliary energy and a 3% reduction in the total cost [20].

Romero-Sánchez et al. [21] evaluated the performance of natural stones with PCM experimentally. They found that the natural stones with PCM had the potential of decreasing the overall energy consumption in the building. Gowreesunker et al. [22] validated a CFD simulation for the performance prediction of a PCM board, which was inserted in a test-cell with the dimensions of 1.3 m × 0.8 m × 1.4 m. Their results showed that the PCM boards could reduce the peak temperature compared to a conventional plasterboard wall. Also, Xu et al. [23] experimentally evaluated latent heat storage consisting of cylindrically micro-encapsulated PCM (Climsel C48) for space heating load regulation. They tested their latent heat storage unit in two tank orientations, namely vertical and horizontal. The comparison results showed that even though PCM charging and discharging time could be shortened up to 20% in the vertical orientation, the PCM thermal capacity reduced to 8.2%.

A prototype house modified with a thin layer of PCM was tested for heat transfer reduction. It was observed that the thin PCM layer, which was a hydrate salt-based PCM, in the most suitable location through the wall could decrease

the heat flux peak up to 29.7% and 51.3% for the west wall and south wall, respectively [24]. Takuç et al. [25] examined PCM utilization in the building elements of a flat roof in Istanbul. They found that some PCM failed to be effective in a climate with four seasons. Afterward, Ye et al. [26] proposed an interesting wall panel of CaCl2.6H2O-Mg (NO3)2.6H2O/expanded graphite composites as PCMs with different melting points due to their mass fractions difference for building energy saving in various seasons. They concluded that one of their proposed PCM had a better performance than the others, indicating the temperature decrement factor of 0.533 and 1.8 h of the temperature lag in a test chamber's thermal behavior. Kant et al. [27] developed ternary mixtures of commercial fatty acids such as Lauric Acid (LA), Capric Acid (CA), Stearic Acid (SA), and Palmitic Acid (PA) in order to prepare PCM for TES application. Among the ternary mixtures developed, 13 ternary mixtures had the potential to be recommended for TES application. Kasaeian et al. [28] reviewed the experimental studies on applying PCMs and Nano-enhanced PCMs in buildings. In another research, they reviewed nanofluid applications on various types of solar energy systems such as photovoltaic, solar thermoelectric, and solar collector [29]. Lin et al. [30] reviewed the thermal performance of thermal energy storage with inorganic PCM.

Nanoparticles have the potential to improve the thermal performance of PCMs. In this regard, Muhammad et al. [31] confirmed that adding nanoparticles to phase change materials amplified the PCM thermal properties to create more energy savings in the building. They analyzed the thermal properties of beeswax as a PCM with high thermal conductivity and a Nano-enhanced-beeswax. The presence of graphene nanoparticles in the beeswax increased the latent heat and heat capacity by 22.5% and 12%, respectively. As another study in this field, Zhu et al. [32] demonstrated that incorporating n-octadecane into expanded perlite composite, fabricating the gypsum board, improved the mechanical and thermal properties. The gypsum board showed the best thermal insulation effect when the dosage of nano-Al2O3 was 0.3 wt.%. Bao et al. [33] developed a PCM cement composite including microencapsulated PCM (MPCM), Nano-silica (NS), and carbon fiber (CF). They concluded that, compared with a cement paste, the functional and structural benefit of cement composite was enhanced by incorporating MPCM, NS, and CF. The phase change temperature ranges of fatty acids make them suitable for TES in buildings as PCM. The low thermal conductivity is a weakness of fatty acids. Martín et al. [34] presented a solution for this problem through the integration of SiO2 nanoparticles with capric acid (CA) and capric myristic acid (CA-MA). The thermal conductivity of CA-MA improved up to 142% after mixing SiO2 nanoparticles with 1.5 wt.%. The effect of nanoparticle diameter and nanoparticle volume fraction on the thermal behavior, and energy consumption of a glazed window, including Nano-PCM, was investigated in different seasons [35]. The researchers concluded that by using Nano-PCM with appropriate particle diameter and volume fraction, the energy consumption decreased to 4%.

As it is well known, using PCM as the latent heat storage in buildings is one of the noteworthy methods to reduce energy consumption. The addition of nanoparticles into the PCM has the potential to improve the thermal performance of the PCMs. The PCM and Nano-enhanced PCM behavior are mainly studied based on a small-scale viewpoint in the existing literature. In this paper, the performance of PCM and Nano-enhanced PCM is analyzed on large-scale wallboard. To better understand the PCM and Nano-enhanced PCM`s impacts on the indoor temperature, three cases, including without PCM, with pure PCM, and with Nano-enhanced PCM, were numerically analyzed. For more accuracy in the solutions, the enthalpy-porosity method in CFD was utilized. The enthalpy-porosity is more complex and accurate compared to the other simulation procedures. Disregarding natural convection in the phase change phenomenon simulation creates significant errors in the modeling results, mainly when PCM is used for a large-scale case. While the enthalpy-porosity method considers this heat transfer mechanism. There are few works published about CFD analyses on the implementation of PCM in large-scale buildings. In this study, the PCM thermal behavior was analyzed on a large scale via CFD. Also, as a novel methodology, the thermal behavior of indoor airflow and PCM was investigated simultaneously.

METHODOLOGY

The numerical study consists of the formulation and characterization of the PCM and Nano-enhanced PCM, which are implemented in the southern wall of a room as wallboard. Also, the room's thermal behavior, using PCM and Nano-enhanced PCM, is investigated. The details are described below.

Description of the System and Physical Model

Since this study aims to investigate the ability to use PCM and Nano-enhanced PCM for reducing energy consumption, a room without a door and window is considered. Fig. 1 shows the room geometry in 2D. The walls of the pre-modified room comprise concrete, gypsum, and brick.

Table 1 represents the physical properties of construction materials. The PCM is located in the southern wall of the room due to the highest solar radiation. The southern wall has a 15 cm thickness, while the thickness of PCM is 2 cm. When the southern wall without PCM is simulated, gypsum with the same thickness would be considered instead of the PCM.

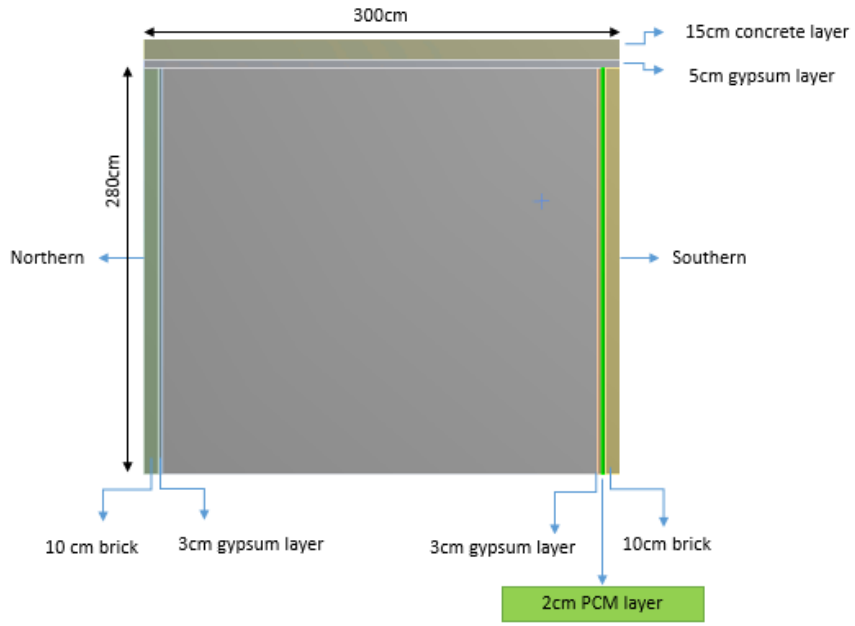

Figure 1. The geometry of the case study.

Table 1. Physical properties of materials for constructing the reference room

Material	k (W $m^{-1}K^{-1}$)	C (J $kg^{-1}K^{-1}$)	ρ (kg m^{-3})
Concrete	1.25	1200	2300
Brick	0.7	840	1600
Gypsum	0.5	1000	1200

Mathematical Formulation

This study's used heat transfer mechanisms include the conduction heat transfer for solid materials such as concrete, brick, gypsum, and PCM in the solid phase and the convection heat transfer for the ambient air and PCM in the liquid phase. The PCM in the liquid phase has both convection and conduction heat transfer; furthermore, due to the difference in the density of its two phases, the laminar flow equations are considered for the liquid phase of this case. The following assumptions are considered for modeling:

- The PCM in the liquid phase is an incompressible and Newtonian fluid.
- The flow regime in the PCM in the liquid phase is considered as laminar flow.
- Constant thermo-physical properties are considered, except for the PCM thermo-physical properties, which vary with the temperature.
- The heat conduction process in the wall layers is one-dimensional
- The volume difference caused by phase change is negligible
- Convection heat transfer in the liquid phase of PCM is considered two-dimensional
- Convection heat transfer in the ambient air is considered two-dimensional
- Viscous dissipation in the liquid PCM is negligible

- Governing Equations of Solid Materials

The energy equation for the solid materials used in the building structure and solid PCM is presented as Eq. 1. The thermal conductivity coefficient, density, and specific heat capacity in constant pressure is assumed constant in this equation.

$$\rho C_p \frac{\partial T}{\partial t} = \frac{\partial}{\partial x}\left(k\frac{\partial T}{\partial x}\right) + \frac{\partial}{\partial y}\left(k\frac{\partial T}{\partial y}\right) \quad (1)$$

In the above equation, C_p(J/kg.K), k(W/m.K), and T(K) are the specific heat capacity, thermal conductivity, and temperature, respectively.

- Governing Equation for Phase Change

The enthalpy-porosity method is considered for the PCM. The governing equations on the melting phenomenon, corresponding to the above assumptions and using the Boussinesq model are demonstrated as followings:

- Continuity equation:

$$\frac{\partial u}{\partial x} + \frac{\partial v}{\partial x} = 0 \quad (2)$$

- Momentum equations:

$$\frac{\partial}{\partial t}(\rho u)+\frac{\partial}{\partial x}(\rho uu)+\frac{\partial}{\partial y}(\rho vu)=-\frac{\partial p}{\partial x}+\frac{\partial}{\partial x}\left(\mu\frac{\partial u}{\partial x}\right)+\frac{\partial}{\partial y}\left(\mu\frac{\partial u}{\partial y}\right)+S_x \quad (3)$$

$$\frac{\partial}{\partial t}(\rho v)+\frac{\partial}{\partial x}(\rho uv)+\frac{\partial}{\partial y}(\rho vv)=-\frac{\partial p}{\partial y}+\frac{\partial}{\partial x}\left(\mu\frac{\partial v}{\partial x}\right)+\frac{\partial}{\partial y}\left(\mu\frac{\partial v}{\partial y}\right)+F_b+S_y \quad (4)$$

Here, F_b is the buoyancy force, which can be obtained from the Boussinesq approximation [36]:

$$F_b = \rho_{liquid} g(1 - \beta(T - T_m)) \quad (5)$$

Where g is the acceleration due to gravity, T_m is the PCM melting temperature, β is the thermal expansion coefficient, and ρliquid is the density of PCM, when it is in the liquid phase.

Also, S_x and S_y (Pa/m) are a source term vector, which is added to the above equations for modeling of natural convection in the porous phase of PCM [37].

$$S_i = A_{mushy}\frac{(1-\gamma(T))^2}{(\gamma(T)^3-\varepsilon)}\vec{u} \quad (6)$$

Where ε has a small amount about 0.001 to prevent being zero the denominator, A_{mushy} (kg/m^3.s) is the porosity function which is equivalent to 10^5 [38], $\vec{u}$ is the velocity component, and γ(T) is the liquid fraction:

$$\gamma = \frac{\Delta H}{L} \quad (7)$$

Where ΔH (J/kg) is the latent heat content which is variant between zero in the solid phase to 1 for the liquid phase of PCM, and L (J/kg) is latent heat of phase change. The amount of γ(T) is given by the following equation:

$$\gamma(T)=\begin{cases}0 & T<T_m-\Delta T\\ (T-T_m+\Delta T)/2\Delta T & T_m-\Delta T<T<T_m+\Delta T\\ 1 & T>T_m+\Delta T\end{cases} \quad (8)$$

Where T_m (K) is the PCM's melting temperature, and ΔT is the half range of the melt temperatures. The γ(T) is 1 when the PCM is in the liquid phase, and zero when this is in the solid phase. It linearly grows from zero to 1 between the solid and liquid phases [39].

The energy equation considering latent heat transfer and storage and is expressed as below:

$$\frac{\partial}{\partial t}(\rho H)+\frac{\partial}{\partial x}(\rho uH)+\frac{\partial}{\partial y}(\rho vH)=\frac{\partial}{\partial x}\left(k\frac{\partial T}{\partial x}\right)+\frac{\partial}{\partial y}\left(k\frac{\partial T}{\partial y}\right) \quad (9)$$

Where k (W/m.K) is the thermal conductivity, T is the temperature fraction, and H is the total energy divided into the volume, which is calculated by the following equation:

$$H = h + \Delta H \quad (10)$$

Where h (J/kg) is the sensible enthalpy, and ΔH is the latent heat content [40]. The amount of h is calculated by employing the following equation:

$$h = h_{ref} + \int_{T_{ref}}^{T} C_p dT \quad (11)$$

Where T_{ref} = 298.15 K and h_{ref} (J/kg) and C_p(J/ kg.K) are enthalpy in the reference temperature and specific heat, respectively [37].

By placing H in the energy equation, this equation is generally written as follows to the non-isothermal phase change:

$$\frac{\partial}{\partial t}(\rho C_P T)+\frac{\partial}{\partial x}(\rho u C_P T)+\frac{\partial}{\partial y}(\rho v C_P T)=\frac{\partial}{\partial x}\left(k\frac{\partial T}{\partial x}\right)+\frac{\partial}{\partial y}\left(k\frac{\partial T}{\partial y}\right)-\frac{\partial}{\partial t}(\rho\Delta H)+\frac{\partial}{\partial x}(\rho u\Delta H)+\frac{\partial}{\partial y}(\rho v\Delta H) \quad (12)$$

The above energy equation can be used in solid, liquid and two-phase regions according to the liquid fraction values that will be obtained by solving simultaneously with the energy equations.

- Governing Equations for the PCM Enhanced with Nanoparticle

The thermo-physical equations of the Nano-enhanced PCM are similar to the nanofluid equations when the PCM in the liquid phase is used as the basic fluid. The following assumptions are considered for the Nano-enhanced PCM analysis:

- The Nano-enhanced PCM enhanced in the liquid phase is Newtonian and incompressible.
- The volumetric expansion of the solid nanoparticles is negligible.
- The thermo-physical properties of the PCM are assumed time dependent.

- The nanoparticles are homogeneously distributed in the PCM.
- The flow of the PCM in the liquid phase is laminar, and viscous dissipation is negligible.

The Nano-enhanced PCM density is presented by the following equations [41]:

$$\rho_{NePCM} = (1 - \varphi)\rho_{PCM} + \varphi\rho_{np} \quad (13)$$

$$\rho_{PCM}(T) = \rho_S + (\rho_l - \rho_s)\,\gamma(T) \quad (14)$$

Where ρ_{PCM}(kg/m^3) and ρ_{np}(kg/m^3) are the total density of PCM and solid nanoparticles, respectively, φ is the volume fraction of the nanoparticles, and ρ_s and ρ_l are the PCM densities in solid and liquid phases, respectively. The heat capacity of the Nano-enhanced PCM is calculated by the following equation [41]:

$$(\rho C_p)_{NePCM} = (1 - \varphi)(\rho C_p)_{PCM} + \varphi(\rho C_p)_{np} \quad (15)$$

Also, Nano-enhanced PCM`s viscosity is determined by Eq. 15 [42]:

$$\mu_{NePCM} = \frac{\mu_{PCM}}{(1-\varphi)^{2.5}} \quad (16)$$

Where μ_{PCM} (m^2/s) is the PCM viscosity when it is in the liquid phase. Also, the latent heat of Nano-enhanced PCM is [41]:

$$L_{NePCM} = \frac{(1-\varphi)(\rho L)_{PCM}}{\rho_{NePCM}} \quad (17)$$

Where L_{PCM} (J/kg) is the latent heat of PCM.

The thermal conductivity of Nano-enhanced PCM was determined using the Maxwell model [43]:

$$k_0 = k_{PCM}\frac{k_{np} + 2k_{PCM} - 2\varphi(k_{PCM} - k_{np})}{k_{np} + 2k_{PCM} + \varphi(k_{PCM} - k_{np})} \quad (18)$$

$$k_{PCM}(T) = k_S + (k_l - k_s)\,\gamma(T) \quad (19)$$

Where k_{PCM}, k_{np}, k_S and k_l (W/m.K) are the thermal conductivities of PCM, nanoparticle, solid PCM and liquid PCM, respectively. The effective thermal conductivity of the Nano-enhanced PCM is:

$$k_{NePCM} = k_d + k_0 \quad (20)$$

$$k_d = 5\times10^4\beta_k\,\xi\varphi(\rho C_P)_{PCM}\sqrt{\frac{B_0 T}{\rho_{np} d_{np}}}f(T,\varphi) \quad (21)$$

Where d_{np} is the nanoparticles diameter, B_o is the Boltzmann constant (1.381 × 10^{-23} J/K), β_k = 8.4407(100ϕ)$^{-1.07304}$, and ξ is a correction factor, which is dependent on the liquid fraction, γ(T) in Eq. 7.

Boundary Conditions

In this paper, heat transfer between the indoor and ambient occurs only at the southern wall and the ceiling. The governing equations correspond to the boundary condition at the southern wall and ceiling, shown in Figs. 2–3, can be described by the following equation:

$$-k\frac{\partial T}{\partial x} = \alpha q_{solar} + h_o(T_{amb} - T_s) + \varepsilon\sigma(T_{amb}^4 - T_{os}^4) \quad (22)$$

Where α is the solar absorption coefficient for the wall's external surfaces, which is considered as 0.65 [44], q_{solar} (W/m^2) is the incident solar radiation which is calculated based on the case location, wall direction, day data and hour, and h_o (W/m.K) is the exterior convective heat transfer coefficient [45]:

$$h_o = 18.6U_s^{0.605}, \quad U_S = 0.5 \quad \text{for} \quad U_{10} < 2\text{m/s} \quad (23)$$

The boundary condition, related to the other walls except of southern wall and roof, is assumed as isolation $\left(\frac{\partial T}{\partial x} = 0\right)$. Also, the boundary condition for the external surfaces of the southern wall and roof is presented as the following equation:

$$k\frac{\partial T}{\partial x} = h_i(T_{in} - T_{is}) \quad (24)$$

Where h_i is interior convective heat transfer coefficient:

$$h_i = Nu\frac{k}{L_c} \quad (25)$$

$$Nu = c\,Ra^m \quad (26)$$

Regarding the above equation, Nu number has a direct relation to the Rayleigh number. The Rayleigh number is reported as 10^7 considering the geometry and boundary condition of the problem, which is given by:

$$Ra = \rho g\beta L_C(T_H - T_C)/\alpha\mu \quad (27)$$

Where c and m are constant coefficients whose values are dependent on the geometry and boundary conditions.

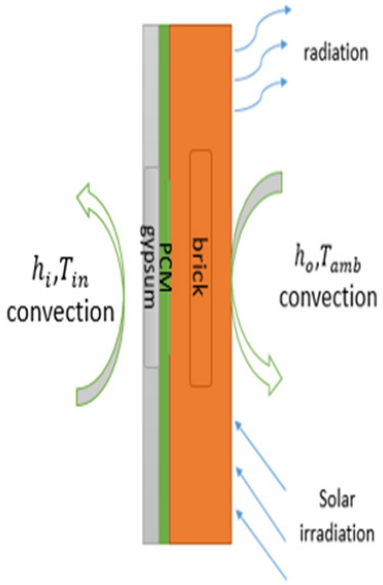

Figure 2. Boundary condition of the south wall.

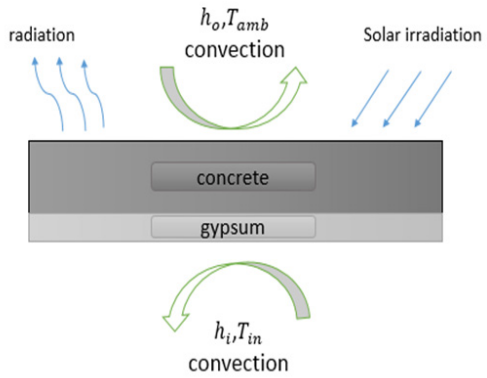

Figure 3. Boundary condition of the roof.

Mesh Independency Test

Fig. 4 shows the structured and uniform mesh generated in ANSYS meshing, which is used for all the reported numerical simulation cases.

The numerical model consists of 66920 elements, while the stratification meshing is used for the wall domain due to more accuracy. To ensure that a mesh-independent solution would be obtained, the results from this model are compared with the results of numerical models with a different number of elements as 31800, 66020, and 102527 elements. The acquired results showed that the difference between the results is less than 1%. Hence, the origin model is adopted from the numerical simulation. Table 2 presents the results of the model`s meshing comparison.

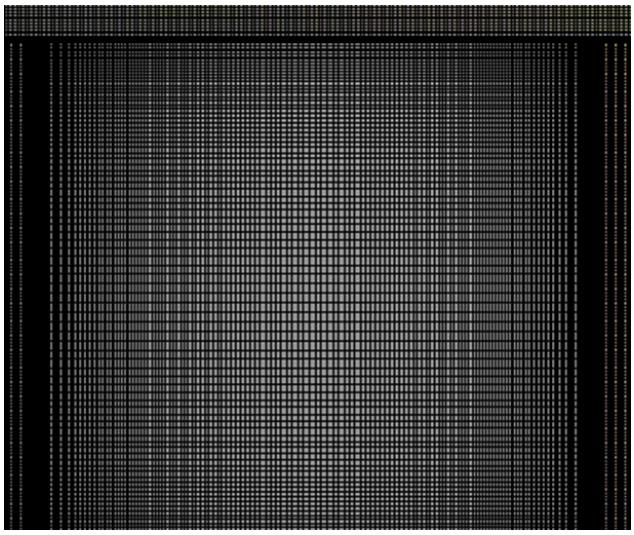

Figure 4. Geometry of meshing.

Table 2. The acquired results of mesh independency test

Number	Elements number	Temperature (°C)
1.	31800	27.42
2.	66020	28.079
3.	102527	28.084

MODEL OF VERIFICATION

In order to ensure that the computational procedure is accurate enough, the acquired results from the simulation are verified by the experimental results achieved by Alqallaf and Alwadhi [46]. They carried out a thermal analysis on a concrete roof with vertical cylindrical holes, filled with three types of paraffin, provided from the PlusICE Company in UK, with different melting temperatures as the PCM A32, PCM A28, and PCM A39. The width and length of the concrete slab are 1.5 m, and its thickness is 0.15 m. The vertical cylindrical holes' height and diameter are equal to 0.075 m and 0.1414 m, respectively. A model of the concrete with cylindrical holes was simulated, then its results were compared with the results of Alqallaf and Alwadhi. Fig. 5 presents the comparison of the interior surface temperature between the simulation and experimental study results.

It is evident from Fig. 5 that there is a good match between the experimental and numerical results with a maximum error of 7.83%. The little difference between the experimental and the obtained numerical results is the absorption coefficient, indoor convection heat transfer coefficient, and convection heat transfer of the ambient, which have been assumed constant in the simulation.

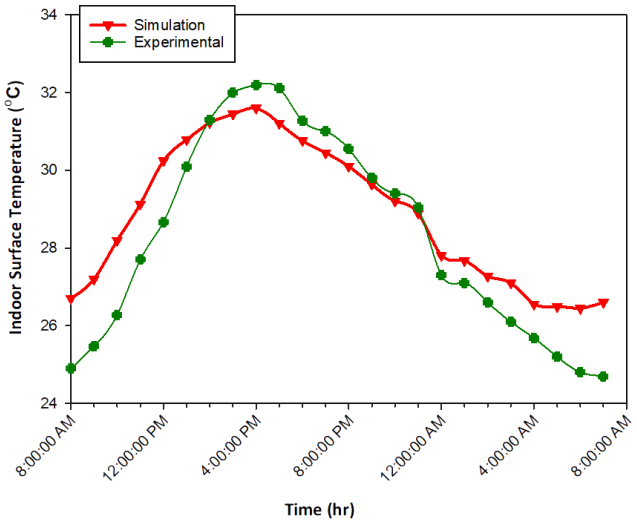

Figure 5. Verification of the interior temperature.

RESULTS AND DISCUSSION

In the following sub-sections, PCM and Nano-enhanced PCM simulation results as wallboard in a room are collected. In general, insertion PCM in the room's southern wall has advantages in thermal regulation and decreasing the temperature fluctuations. Moreover, the implementation of nanoparticles into the PCM amplifies the PCM thermal performance.

Climatic Conditions

In the Tehran climate, September is one of the warmest months of the year. Furthermore, the selected PCM should be melted during the day, which effectively works in a high ambient temperature. Hence, the numerical test is conducted in September in the Tehran climate.

The ambient temperature and solar irradiation, as shown in Figs. 6 and 7, are two variant parameters.

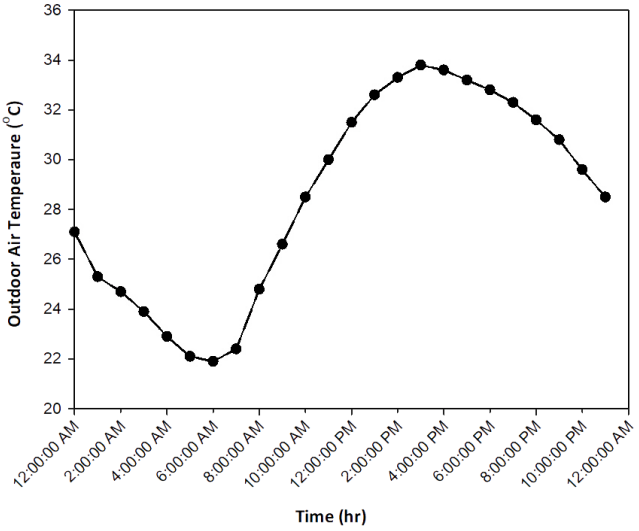

Figure 6. Ambient temperature in Tehran (1st September).

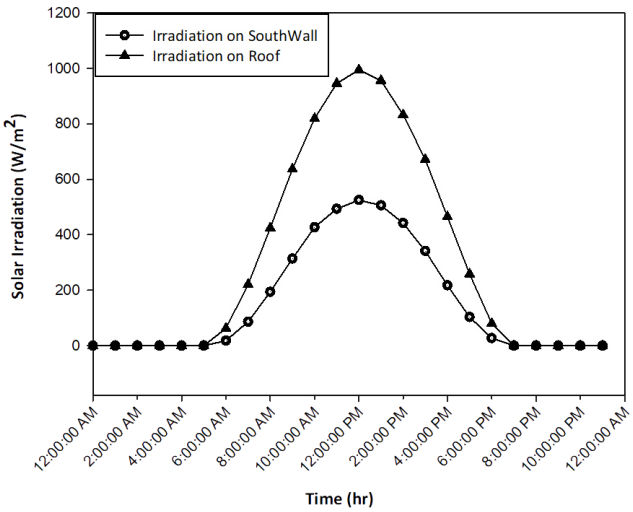

Figure 7. Solar radiation in Tehran on a summer day.

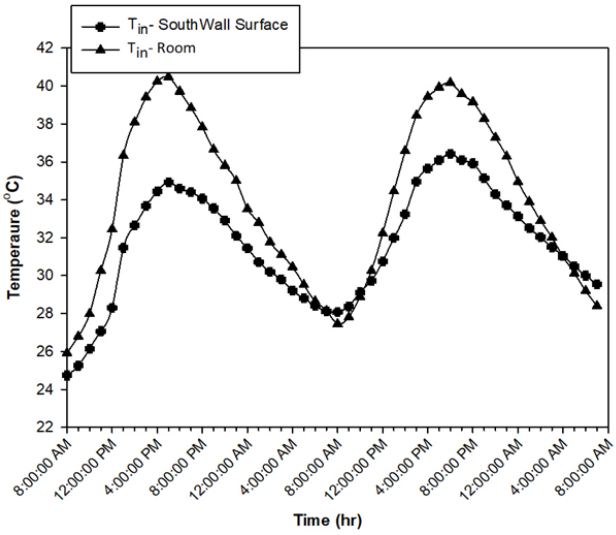

Figure 8. Temperature of the indoor and southern wall surfaces of room.

The simulations were performed on two consecutive days to achieve sustainable results; then, the second day's obtained results were reported due to more balance. First, the room was modeled without PCM. Fig. 8 depicts the room temperature without PCM on two consecutive days. At the beginning of the simulation on the first day, the indoor temperature is assumed 24 °C. As shown in Fig. 8, the difference between the first and second days is the hypothetical situation at the beginning of the simulation. Indeed, in the account of various references, the obtained results of the second day are more reliable [27, 28]. The minimum indoor temperature is 28 °C at 8 am, and the maximum indoor temperature is 36.42 at 6 pm. In addition, the interior surface temperature of the southern wall is also shown in Fig. 8.

Effect of Adding PCM

According to the previous studies [20, 29], a type of organic paraffin with a melting temperature of 28°C was selected as a PCM that was both close to the comfort temperature range temperature (22–28°C) and close to average ambient temperature during the day. It should be noted that the PCM melting temperature was preferred to be closer to the room temperature [50]. The PCM properties are reported in Table 3.

Fig. 9 represents a comparison between the average indoor temperate and temperature of southern wall's interior surface with and without PCM. The southern wall temperature has a significant reduction from 11 am to around 2 am, within the peak demand hours, 15.11% or 6 °C, when the PCM is placed in the wall. Also, the wall surface temperature reaches the maximum, one hour later than the case without PCM. Also, from about 2 am to the early hours of the morning, when the ambient temperature decreases, the wall temperature with PCM is higher than without PCM, but this temperature difference is much less than during peak hours; this is related to the difference in the heat flux of the inner surface of the wall in these two cases.

Fig. 10 presents the interior surface heat flux. In this Figure, the negative amount of heat flux and the positive amount indicate heat absorption and heat release. The PCM wall absorbs heat from both ambient and indoor at the peak hours. At these hours, due to the higher temperature of the indoor, as shown in Figs. 6 and 8, heat absorption by the PCM from the indoor is more than the heat absorption from the ambient. Consequently, the interior surface of the southern wall has a lower temperature compared to the room wall without PCM.

The wall with PCM transfers heat to the indoor room by its phase change from liquid to solid state along night time. While, at the same time, the wall without PCM transfers heat from the indoor to the outdoor because the indoor temperature is higher than the ambient temperature. The difference between the wall heat flux, with and without PCM, is measured by almost 21.67 W/m2 at day and 9.21 W/m2 along the night. According to the previous discussion, it can be seen in Fig. 9 that the temperature difference in the peak is higher in comparison to it at the non-sunshine hours. Also, in the case of PCM, a reduction in the indoor peak temperature is observed by about 4.17% or 1.52°C, in the peak hours, between 11 am to around 10:30 pm, as shown in Fig. 9. Moreover, reaching the peak temperature of the indoor temperature has an approximate delay of 45 min. Furthermore, the temperature fluctuations decrease by about 31.11%.

Table 3. Thermo-physical properties of PCM, Al_2O_3, and nano-enhanced PCM

Property		PCM	Al_2O_3	PCM + 2%Al_2O_3
Melting temperature (°C)		27–29		28
Latent heat (kJ/kg)		245		
Thermal conductivity (W/m.K)	Solid	0.35	36	0.22
	Liquid	0.149		
Density (kg/m^3)	Solid	814	3600	831.5
	Liquid	775		
Specific heat (kJ/kg.K)	Solid	1.93	765	1893
	Liquid	2.16		
Kinematic viscosity (m^2/s)		5×10^{-6}		4.8×10^{-6}
Thermal expansion (1/K)		9.1×10^{-4}		8.3×10^{-4}
Nanoparticle diameter (m)			59×10^{-9}	

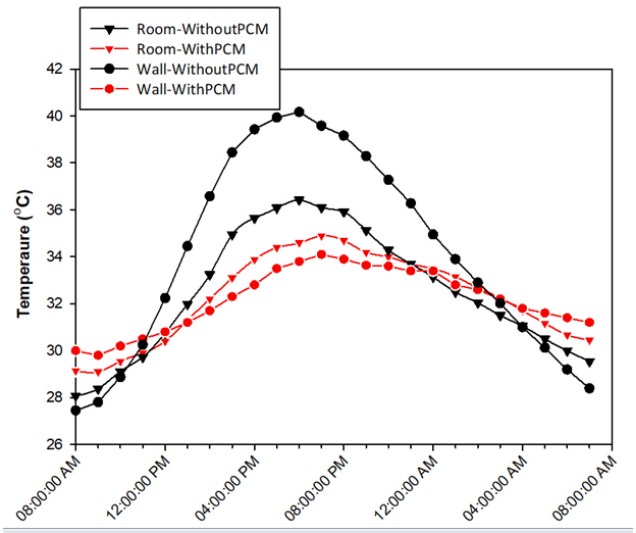

Figure 9. The average indoor temperature and the interior surface temperature, with and without PCM.

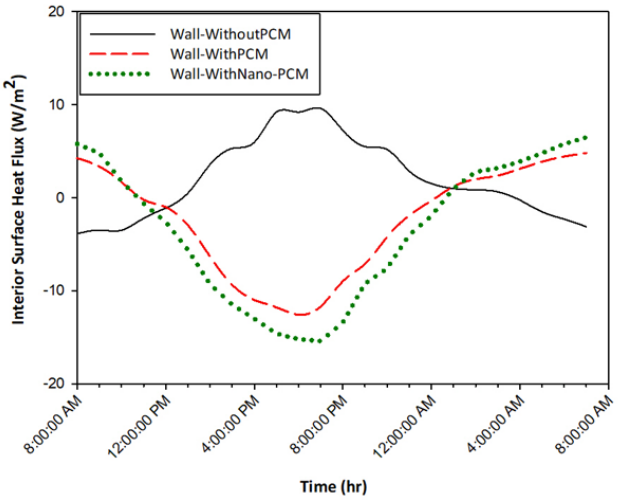

Figure 10. The interior surface heat flux, with and without PCM and with Nano-PCM.

Effect of Adding Nanoparticle to PCM

In this section, in order to improve the PCM's thermo-physical properties and increase the PCM performance in the building, Al_2O_3 solid nanoparticles are distributed in the PCM. Regarding the previous literature, in order to model the Nano-enhanced PCM, simulation of the solid nanoparticles is neglected. Hence, the Nano-enhanced PCM is modeled based on the amplified properties of the PCM. Table 3 shows the calculated properties of the PCM modified with 2% Al_2O_3.

As shown in Fig. 10, the negative value of heat flux, which is absorbed by the Nano-enhanced PCM, increases to 34.52 W/m^2 higher than the case with pure PCM. Conversely, the heat released from Nano-enhanced PCM wall is higher by about 6.42 W/m^2 than the case with pure PCM at the night time.

The melting rate in Nano-enhanced PCM is higher than that of pure PCM, as shown in Fig. 11. The addition of nanoparticles into the PCM affects its thermal properties, increasing the thermal conductivity and decreasing the latent heat of fusion. Hence, the Nano-enhanced PCM absorbs more heat than pure PCM; consequently, the Nano-enhanced PCM melts earlier than pure PCM.

In addition, to better understand the difference between the melting rate of the PCM and Nano-enhanced PCM, the contours related to the liquid fraction of both PCM and Nano-enhanced PCM, at 8 am, 2 pm, and 8 pm, respectively, are shown in Fig. 12. As it can be seen, the maximum difference between the liquid fraction of PCM and Nano-enhanced PCM is occurred at 8 am.

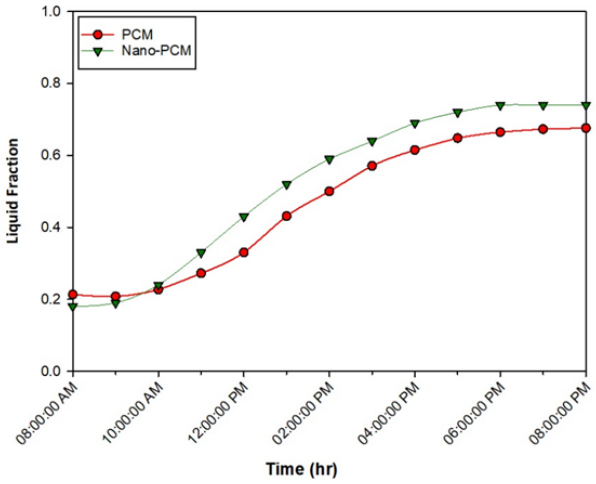

Figure 11. Liquid fraction in pure PCM and Nano-enhanced PCM.

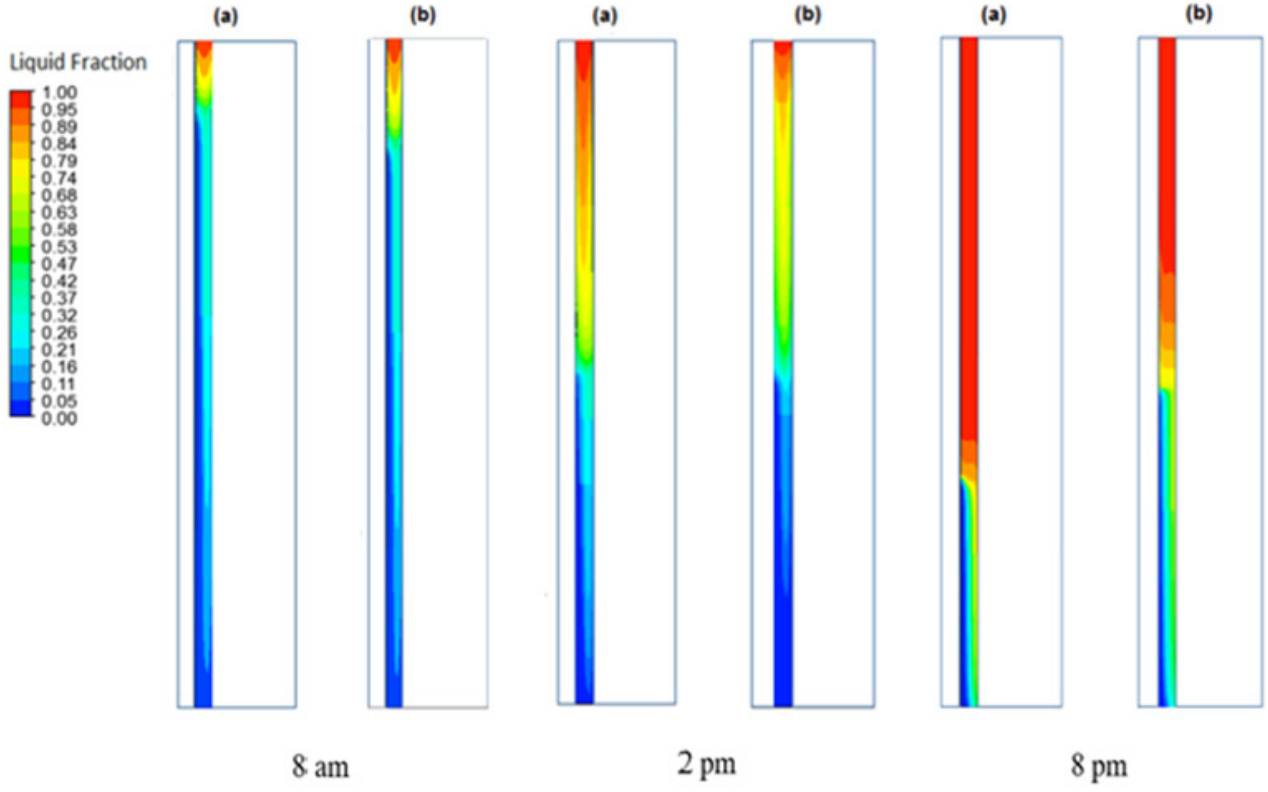

Figure 12. Liquid fraction contours of (a) Nano-enhanced PCM, (b) Pure PCM.

COMPARISON RESULTS

The difference between heat absorption and heat release is because of the addition of nanoparticles to the PCM. This process increases the PCM thermal conductivity and decreases the PCM latent heat of fusion; accordingly, the heat transfer and the velocity of melting and solidification in Nano-enhanced PCM is more than that of pure PCM.

In the Nano-enhanced PCM case, the indoor temperature within the heat release hours is more than pure PCM one due to the heat transfer enhancement. On the contrary, the indoor temperature of Nano-enhanced PCM is lower than the indoor temperature in the case of PCM in the heat absorption hours, as shown in Fig 13. Furthermore, when Nano-enhanced PCM is implemented in the wall, temperature fluctuations are 52% and 31% lower than with PCM and without PCM, respectively.

Fig. 14 illustrates the indoor temperature counters in the three cases; without PCM, with PCM, and with Nano-enhanced PCM. It can be clearly seen the difference in indoor temperature in these three cases when reaching the peak temperature.

Fig. 15 shows the differences between the wall's interior surface temperature with PCM, Nano-enhanced PCM, and without PCM for 24 hours. The maximum amount of interior surface temperature is increased by about 1.5 °C, and the minimum temperature of the interior surface is decreased by about 0.4 °C. In addition, the fluctuation of indoor temperature is reduced by 1.86 °C, roughly 43.25 %. The fluctuations of the temperature of the interior surface are decreased roughly 10.2 °C or 80.42 %.

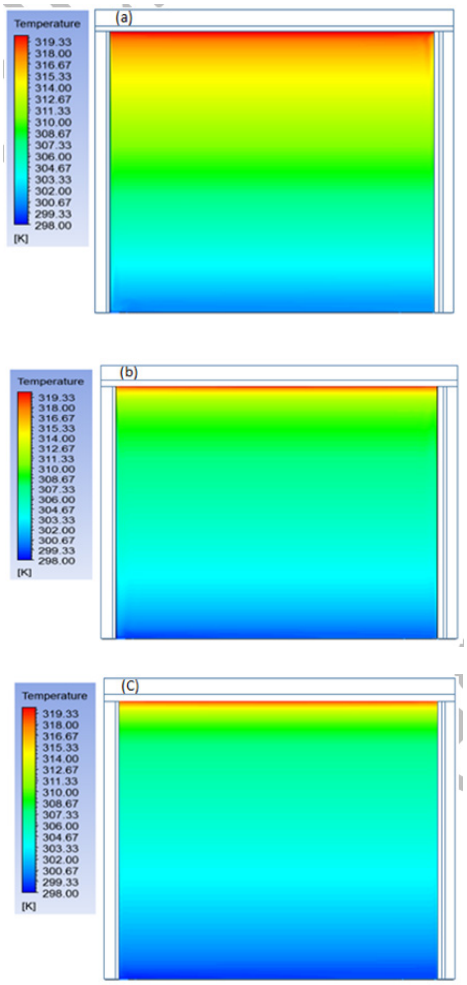

Figure 14. Comparison of the indoor temperature counters for the maximum temperature in: (a) without PCM, (b) with PCM, (c) with Nano-enhanced PCM.

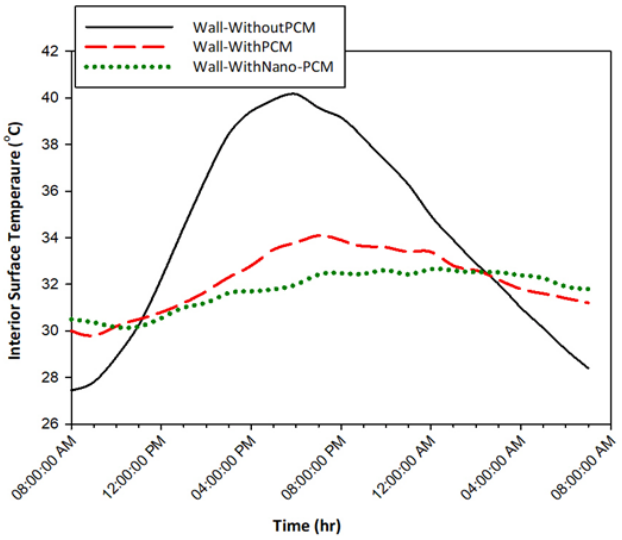

Figure 13. The average indoor temperature for PCM, Nano-enhanced PCM, and without PCM.

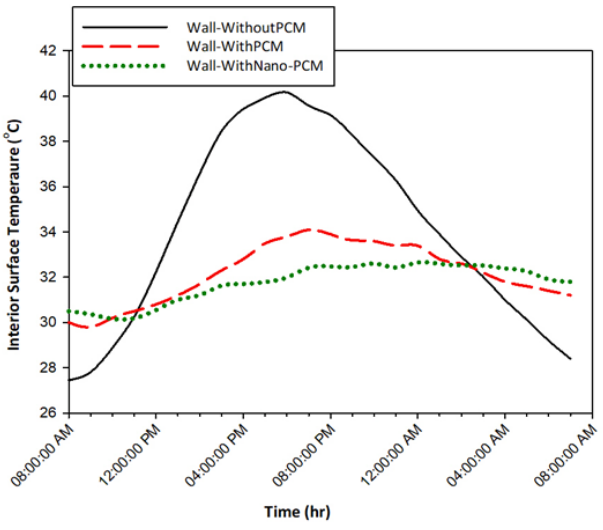

Figure 15. The interior surface temperature of the wall for PCM, Nano-enhanced PCM, and without PCM.

There are three factors for evaluating the performance of the PCM, which is implemented in the wall, including the temperature-time lag, the temperature decrement factor, and the energy storage:

$$\varphi_{PCM} = t_{PCM,\,max} - t_{air,\,max} \tag{28}$$

$$f_{PCM} = \frac{T_{PCM,max} - T_{PCM,min}}{T_{air,max} - T_{air,min}} \tag{29}$$

$$\eta = \frac{Q_{air} - Q_{PCM}}{Q_{air}} \tag{30}$$

Where Q_{air} and Q_{PCM} are energy consumption by the air-conditioning system in the cases of without PCM and with PCM wallboard, respectively. In this study, the reference temperature is assumed 297.15 K. The air conditioning`s energy consumption is calculated by:

$$Q = \sum_{t=1}^{24} MC_p \left| T_R - 297.15 \right| \tag{31}$$

Where M is assumed as 1.2 kg/s.

The energy consumption of air-conditioning system for reaching the set-point in three cases are illustrated in Fig. 16. Also, Table 4 shows the values related to three mentioned factors and total energy consumption of the air-conditioning system.

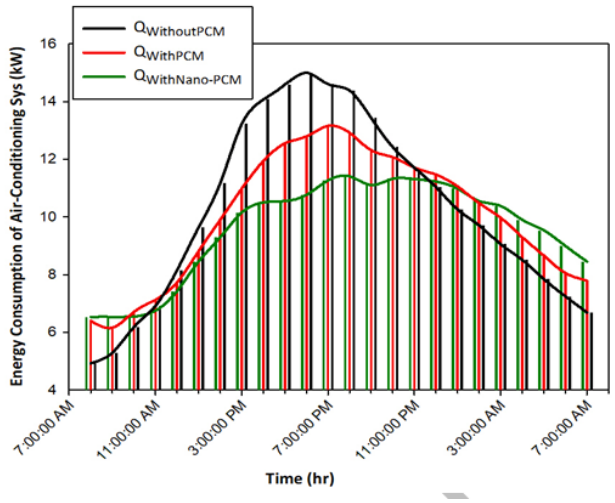

Figure 16. Energy consumption of air-conditioning.

The total energy consumption by the air-conditioning system during a day in the case of Nano-enhanced PCM is about 4.5 % and 7.4 % lower than that of pure PCM and without PCM, respectively. From Table 4 it can be concluded that the thermal performance of the room is directly related to the temperature-time lag and energy storage; however, it has an inverse relationship with the temperature decrement factor. The case with Nano-enhanced PCM reaches the more temperature-time lag by 21.6 min, about 4.37% higher energy storage, compared to the case of pure PCM.

CONCLUSION

This paper's objective is a comparison between thermal performance of pure PCM and Nano-enhanced PCM as wallboard in a room in the Tehran climate. For this purpose, a numerical simulation is carried out through CFD methods on a large scale. Melting temperature is one of the most important and effective factors in the thermal performance of PCM, so in choosing PCM, it should be noted that its melting temperature is close to the thermal comfort temperature range and the average ambient temperature during the day; otherwise, it cannot be possible to take maximum advantage of PCM's latent heat. Also, it must be pointed out that since the selected PCM does not completely melt or solidify during a summer day due to the low-temperature difference between day and night, its thermal performance seems to be lower than expected.

From the simulation results, the following conclusions are reported:

- Using PCM led to decreasing the maximum temperature and increasing the minimum temperature; consequently, decreasing the temperature fluctuations. It could be noted that increasing the minimum temperature was significantly lower than decreasing the maximum temperature.
- In using PCM, the heat absorption from interior space led to a decrease in the interior temperature and temperature fluctuations.
- The interior temperature was near to the PCM melting temperature, so the heat transfer from PCM to the room, at midnight, was lower than the heat absorbed from the interior space by PCM.
- The addition of nanoparticles to the PCM improved the thermo-physical properties of PCM. This issue

Table 4. Thermal performance indices of the PCM on the room

Room type	t_{max}(hr)	φ_{PCM}(min)	T_{max}(K)	T_{min}(K)	f_{PCM}	Q(kW)	η(%)
Without PCM	18		309.57	301.15		240.23	
With PCM	18.75	45	308.5	302.25	0.742	232.93	3.03
With Nano-enhanced PCM	19.11	66.6	306.52	302.56	0.470	222.44	7.4

caused increasing the melting rate by increasing the thermal conductivity and decreasing PCM's latent heat of fusion.
- The high melting and solidification rates in Nano-enhanced PCM increased the heat transfer through the heat storage process.
- The temperature fluctuations were reduced by 52% and 31% by utilizing Nano-enhanced PCM and pure PCM, respectively.
- The total energy consumption by the air-conditioning system during a day in the case of Nano-enhanced PCM wallboard is 4.5% and 7.4% less than the case of pure PCM and room without PCM, respectively.
- The use of Nano-enhanced PCM postponed the peak temperature by 21.6 min more than the pure PCM, and also performed better with 4.37% more energy storage.

AUTHORSHIP CONTRIBUTIONS

Authors equally contributed to this work.

DATA AVAILABILITY STATEMENT

The authors confirm that the data that supports the findings of this study are available within the article. Raw data that support the finding of this study are available from the corresponding author, upon reasonable request.

CONFLICT OF INTEREST

The author declared no potential conflicts of interest with respect to the research, authorship, and/or publication of this article.

ETHICS

There are no ethical issues with the publication of this manuscript.

REFERENCES

[1] Energy efficiencyThe first fuel of a sustainable global energy system. Available from: https://www.iea.org/topics/energyefficiency/buildings/. Accessed on May 13, 2019.

[2] Sonker VK, Chakraborty JP, Sarkar A, Singh RK. Solar distillation using three different phase change materials stored in a copper cylinder. Energy Rep 2019;5:1532–1542. [CrossRef]

[3] Ghadbeigi L, Day B, Lundgren K, Sparks TD. Cold temperature performance of phase change material based battery thermal management systems. Energy Rep 2018;4:303–307. [CrossRef]

[4] Zhu N, Ma Z, Wang S. Dynamic characteristics and energy performance of buildings using phase change materials: A review. Energy Convers 2009;50:3169–3181. [CrossRef]

[5] Sharma A, Tyagi VV, Chen CR, Buddhi D. Review on thermal energy storage with phase change materials and applications. Renew Sust Energ Rev 2009;13:318–345. [CrossRef]

[6] Hariri AS, Ward I.C. A review of thermal storage systems used in building applications. Build Environ 1998;23:1–10. [CrossRef]

[7] Gracia A De, Rincon L, Castell A, Jimenez M, Boer D, Medrano M, et al. Life Cycle Assessment of the inclusion of phase change materials (PCM) in experimental buildings. Energy Build 2010;42:1517–1523. [CrossRef]

[8] Baetens R, Jelle BP, Gustavsen A. Phase change materials for building applications: A state-of-the-art review. Energy Build 2010;42:1361–1368. [CrossRef]

[9] Diaconu BM, Cruceru M. Novel concept of composite phase change material wall system for year-round thermal energy savings. Energy Build 2010;42:1759–1772. [CrossRef]

[10] Kuznik F, Virgone J, Johannes K. In-Situ Study of Thermal Comfort Enhancement in a Building Equipped with Phase Change Material Wallboard. Renew Energy 2011;36:1458–1462. [CrossRef]

[11] Choubineh N, Jannesari H, Kasaeian A. Experimental study of the effect of using phase change materials on the performance of an air-cooled photovoltaic system. Renew Sust Energy Rev 2019;101:103–111. [CrossRef]

[12] Amirifard M, Kasaeian A, Amidpour M. Integration of a solar pond with a latent heat storage system. Renew Energy 2018;125:682–693. [CrossRef]

[13] Kladisios P, Stegou-Sagia A. Using phase change materials in photovoltaic systems for cell temperature reduction: a finite difference simulation method. J Therm Eng 2016;2:897–906. [CrossRef]

[14] Bai Y, He X, Liu Y, Duan J, Wang Y, Han X. Experimental investigation of a solar thermal storage heater assembled with finned heat pipe and collective vacuum tubes. Energy Convers Manag 2018;166:463–473. [CrossRef]

[15] Korti AIN. Numerical simulation on the effect of latent heat thermal energy storage unit. J Therm Eng 2016;2:599–607. [CrossRef]

[16] Zhou T, Xiao Y, Liu Y, Lin J, Huang H. Research on cooling performance of phase change material-filled earth-air heat exchanger. Energy Convers Manag 2018;177:210–223. [CrossRef]

[17] Ben Zohra M, Riad A, Alhamany A, Sennoune M, Mansouri M. Improvement of thermal energy storage by integrating pcm into solar system. J Therm Eng 2020;6:816–828. [CrossRef]

[18] Mousavi S, Kasaeian A, Shafii MB, Jahangir MH. Numerical investigation of the effects of a copper foam filled with phase change materials in a water-cooled photovoltaic/thermal system. Energy Convers Manag 2018;163:187–195. [CrossRef]
[19] Plytaria MT, Tzivanidis C, Bellos E, Antonopoulos KA. Energetic investigation of solar assisted heat pump underfloor heating systems with and without phase change materials. Energy Convers Manag 2018;173:626–639. [CrossRef]
[20] Plytaria MT, Bellos E, Tzivanidis C, Antonopoulos KA. Numerical simulation of a solar cooling system with and without phase change materials in radiant walls of a building. Energy Convers Manag 2019;188:40–53. [CrossRef]
[21] Romero-Sánchez MD, Guillem-Lopez C, Lopez-Buendia AM, Stamatiadou M, Mandilaras I, Katsourinis D, et al. Treatment of natural stones with Phase Change Materials: Experiments and computational. Appl Therm Eng 2012;48:136–143. [CrossRef]
[22] Gowreesunker BL, Tassou SA. Effectiveness of CFD simulation for the performance prediction of phase change building boards in the thermal environment control of indoor spaces. Build Environ 2012;59:612–625. [CrossRef]
[23] Xu T, Chiu JN, Palm B, Sawalha S. Experimental investigation on cylindrically macro-encapsulated latent heat storage for space heating applications. Energy Convers Manag 2019;182:166–177. [CrossRef]
[24] Lee KO, Medina MA, Raith E, Sun X. Assessing the integration of a thin phase change material (PCM) layer in a residential building wall for heat transfer reduction and management. Appl Energy 2015;137:699–706. [CrossRef]
[25] Tokuç A, Başaran T, Yesügey SC. An experimental and numerical investigation on the use of phase change materials in building elements: The case of a flat roof in Istanbul. Energy Build 2015;102:91–104. [CrossRef]
[26] Ye R, Zhang C, Sun W, Fang X, Zhang Z. Novel wall panels containing CaCl2·6H2O-Mg(NO3)2·6H2O/expanded graphite composites with different phase change temperatures for building energy savings. Energy Build 2018;176:407–417. [CrossRef]
[27] Kant K, Shukla A, Sharma A. Ternary mixture of fatty acids as phase change materials for thermal energy storage applications. Energy Reports 2016;2:274–279. [CrossRef]
[28] Kasaeian A, Bahrami L, Pourfayaz F, Khodabandeh E, Yan WM. Experimental studies on the applications of PCMs and nano-PCMs in buildings: A critical review. Energy Build 2017;154:96–112. [CrossRef]
[29] Kasaeian A, Eshghi AT, Sameti M. A review on the applications of nanofluids in solar energy systems. Renew Sust Energy Rev 2015;43:584–598. [CrossRef]
[30] Lin Y, Alva G, Fang G. Review on thermal performances and applications of thermal energy storage systems with inorganic phase change materials. Energy 2018;165:685–708. [CrossRef]
[31] Amin M, Putra N,. Kosasih EA, Prawiro E, Achmad R, Mahlia T MI. Thermal properties of beeswax/graphene phase change material as energy storage for building applications. Appl Therm Eng 2017;112:273–280. [CrossRef]
[32] Zhu J, Guo B, Hou H, Zhang W. Preparation and Property Modification on Novel Energy Storage Material: n-Octadecane PCMs/Expanded Perlite Composite Gypsum Board. Adv Civ Eng 2019:4501354.
[33] Bao X, Tian Y, Yuan L, Cui H, Tang W, Fung WH. Development of high performance PCM cement composites for passive solar buildings. Energy Build 2019;194:33–45. [CrossRef]
[34] Martín M, Villalba A, Fernández AI, Barreneche C. Development of new nano-enhanced phase change materials (NEPCM) to improve energy efficiency in buildings: Lab-scale characterization. Energy Build 2019;192:75–83. [CrossRef]
[35] Li D, Wu Y, Liu C, Zhang G, Arıcı M. Energy investigation of glazed windows containing Nano-PCM in different seasons. Energy Convers Manag 2018;172:119–128. [CrossRef]
[36] Ebrahimi A, Dadvand A. Simulation of melting of a nano-enhanced phase change material (NePCM) in a square cavity with two heat source–sink pairs. Alex Eng J 2015;54:1003–1017. [CrossRef]
[37] Parsazadeh M, Duan X. Numerical and statistical study on melting of nanoparticle enhanced phase change material in a shell-and-tube thermal energy storage system. Appl Therm Eng 2017;111:950–960. [CrossRef]
[38] Kandasamy R, Wang XQ, Mujumdar AS. Transient cooling of electronics using phase change material (PCM)-based heat sinks. Appl Therm Eng 2008;28:1047–1057. [CrossRef]
[39] Biwole PH, Eclache P, Kuznik F. Phase-change materials to improve solar panel's performance. Energy Build 2013;62:59–67. [CrossRef]
[40] www.FLUENT.com.
[41] Chow LC, Zhong JK, Beam JE. Thermal conductivity enhancement for phase change storage media. Int Commun Heat Mass Transf 1996;23:91–100. [CrossRef]
[42] Vajjha RS, Das DK, Namburu PK. Numerical study of fluid dynamic and heat transfer performance of Al2O3 and CuO nanofluids in the flat tubes of a radiator. Int J Heat Fluid Flow 2010;31:613–621. [CrossRef]
[43] Liu C, Rao Z, Zhao J, Huo Y, Li Y. Review on nano-encapsulated phase change materials: Preparation,

characterization and heat transfer enhancement. Nano Energy 2015;13:814–826. [CrossRef]
[44] Yao J, Yan C. Effects of solar absorption coefficient of external wall on building energy consumption. Proc World Acad Sci Eng Technol 2011;52:682–684.
[45] Defraeye T, Blocken B, Carmeliet J. Convective heat transfer coefficients for exterior building surfaces: Existing correlations and CFD modelling. Energy Convers Manag 2011;52:512–522. [CrossRef]
[46] Alqallaf HJ, Alawadhi EM. Concrete roof with cylindrical holes containing PCM to reduce the heat gain. Energy Build 2013;61:73–80. [CrossRef]
[47] Meng E, Yu H, Zhan G, He Y. Experimental and numerical study of the thermal performance of a new type of phase change material room. Energy Convers Manag 2013;74:386–394. [CrossRef]
[48] Elarga H, Fantucci S, Serra V, Zecchin R, Benini E. Experimental and numerical analyses on thermal performance of different typologies of PCMs integrated in the roof space. Energy Build 2017;150:546–557. [CrossRef]
[49] Ye R, Lin W, Yuan K, Fang X, Zhang Z. Experimental and numerical investigations on the thermal performance of building plane containing CaCl2·6H2O/expanded graphite composite phase change material. Appl Energy 2017;193:325–335. [CrossRef]
[50] Li ZX, Al-Rashed AAAA, Rostamzadeh M, Kalbasi R, Shahsavar A, Afrand M. Heat transfer reduction in buildings by embedding phase change material in multi-layer walls: effects of repositioning, thermophysical properties and thickness of PCM. Energy Convers Manag 2019;195:43–56. [CrossRef]